Journal of
Applied Physics

ARTICLE

scitation.org/journal/jap

Multiphysics simulation of microscale copper printing by confined electrodeposition using a nozzle array

Cite as: J. Appl. Phys. **131**, 055303 (2022); doi: 10.1063/5.0072183
Submitted: 20 September 2021 · Accepted: 6 January 2022 ·
Published Online: 1 February 2022

View Online Export Citation CrossMark

Scott Burlison[1] and Majid Minary-Jolandan[2,a)]

AFFILIATIONS

[1]Department of Mechanical Engineering, The University of Texas at Austin, Austin, Texas 78712, USA
[2]Mechanical and Aerospace Engineering, School for Engineering of Matter, Transport and Energy, Arizona State University, Tempe, Arizona 85287, USA

[a)]**Author to whom correspondence should be addressed:** majid.minary@asu.edu

ABSTRACT

3D printing of metals at the microscale and nanoscale is crucial to produce high-density interconnects and intricate structures in electronic devices. Conventional melting and sintering processes are not suitable for these scales due to a reliance on individual metal particles in the size range of tens of micrometers. Confined electrodeposition (CED) is an established alternative to conventional metal 3D printing processes in which an electrolyte is used to selectively induce deposition of the metal on the printing surface. However, commercialization and efficiency of this process have been limited due to a reliance on sub-micrometer nozzles to achieve desirable deposition rates and single nozzle to achieve uniformity of printed structures. Here, we address these challenges by computationally analyzing an array of microscale nozzles. We tailor the convection within the electrolyte to alter both deposition rate and geometric uniformity of the printed structures. The results show that for large nozzles the evaporation alone is not sufficient to obtain high deposition rates, yet an external pressure can be used to increase deposition and alter uniformity (thickness) of printed structures. Our results can be used to design and analyze new experiments toward parallel multi-nozzle deposition using CED toward high-throughput metal printing.

Published under an exclusive license by AIP Publishing. https://doi.org/10.1063/5.0072183

INTRODUCTION

Metal additive manufacturing (AM) remains one of the most efficient and effective methods to produce complex 3D structures for demanding applications within the aerospace, automotive, and biomedical industries.[1–4] Suitable AM processes for metals are typically based on layer-by-layer deposition through melting/sintering of metal powders, with such processes including selective laser melting (SLM) and direct energy deposition (DED), among others.[5,6] However, such processes are limited to macroscale part production due to a reliance on high working temperatures and individual metal particles in the size range of tens of micrometers.[6–8] Metal AM processes provide an efficient alternative to conventional manufacturing processes at the macroscale, yet AM of metals with microscale resolution has been severely limited. As such, significant interest has recently been spurred in microscale and nanoscale metal AM processes given the anticipated applications in small-scale electronic devices and sensors.[9,10]

Confined electrodeposition (CED) has recently gained attention as an efficient and cost-effective AM process to accurately produce complex metal structures at the microscale and nanoscale.[11,12] Contrary to the typical electrodeposition process in which a conductive material is submerged in an electrolyte bath, CED is a process in which a nozzle containing the electrolyte directly prints the material onto a conductive substrate. Metal deposition at the meniscus tip is a complex multiphysics process in which heat and mass transfer, fluid dynamics, and electrodeposition are simultaneously involved. Among the parameters that affect this process (nozzle size and speed, electric potential, and electrolyte concentration), fluid velocity is a major factor which influences the deposition rate and resulting geometric uniformity of the printed microstructures. Convection is generated within the electrolyte as it flows inside the nozzle toward the cathode. Convective flow affects the ionic flux toward the cathode, thus governing the deposition rate. The fluid velocity can be controlled by altering

Published under an exclusive license by AIP Publishing

the relative humidity of the ambient environment or forcing convection by means of an external pump.

Although CED has been demonstrated experimentally for both a single nozzle[13] and an array of nozzles,[14,15] factors such as evaporation rate and ion flux cannot be sufficiently analyzed *in situ* due to the complex multiphysics phenomena governing the process. Thus, computational models are necessary to fundamentally understand the CED process. Previous studies have developed two-dimensional (2D) finite element (FE) models to study CED for a single nozzle,[16,17] yet no such models have been developed to comprehensively study an array of nozzles printing simultaneously in parallel. Additionally, these studies present results tailored primarily toward nanoscale printing. Parallel printing is necessary to achieve higher throughput for commercialization of this technology. While the underlying physics remain the same for both single and array cases, electrolyte evaporation becomes an even larger issue when studying CED for a nozzle array. For the deposition rate to remain uniform throughout the nozzle array, the evaporation rate on each meniscus surface must be uniform. As the array size increases and the lateral spacing between nozzles decreases, it becomes increasingly difficult for electrolyte to evaporate from the inner nozzles compared to those on the periphery of the array. Metal electrodeposition would then occur at a higher rate for the peripheral nozzles, resulting in non-uniform deposition across the array. Thus, it is of great importance to quantify the effect of array size and nozzle spacing on evaporation rate, ion flux, and deposition rate. In this article, a three-dimensional (3D) finite element (FE) model is developed to investigate the effect of nozzle spacing on such factors for a 3×3 nozzle array for parallel 3D printing of Copper (Cu) structures.

THE MULTIPHYSICS PROCESS

The total flux of ions within the electrolyte depends on convection, diffusion, and migration and is described by the Nernst–Planck equation,

$$N_i = -D_i \nabla c_i - z_i u_i F c_i \nabla \varphi_l + c_i u, \tag{1}$$

in which N_i is the transport vector, D_i is the diffusivity of the chemical species, c_i is the ionic concentration, z_i is the electronic charge of the chemical species, u_i is the velocity of the electrolyte, F is the Faraday constant, and φ_l is the applied electric potential. Boundary conditions for the anode and cathode are charge-transfer reaction kinetics and are described by the Butler–Volmer equation,

$$i_{ct} = i_0 \left(C_R e^{\frac{\alpha_a F \eta}{RT}} - C_O e^{\frac{-\alpha_c F \eta}{RT}} \right), \tag{2}$$

in which i_{ct} is the local current density on the cathode surface, i_0 is the exchange current density, C_R and C_O are the dimensionless concentrations of the reduced and oxidized species, respectively, α_a and α_c are the anodic and cathodic charge-transfer coefficients, respectively, η is the overpotential, R is the universal gas constant, and T is temperature. The first and second terms in Eq. (2) represent the anodic and cathodic components of the local current density, respectively. As deposition occurs, the cathode moves to the tip of the printed structure. The deposition rate on the cathode surface, v_{dep}, is expressed as

$$v_{dep} = -\frac{M_{\mathrm{Cu}} i_{ct}}{z_{\mathrm{Cu}} \rho_{\mathrm{Cu}} F}, \tag{3}$$

in which M_{Cu} is the molar mass of copper and ρ_{Cu} is the copper density.[16–18]

Previous studies have shown that solvent evaporation from the electrolyte meniscus surface has a significant effect on the CED process.[16] Heat and mass transfer must be accounted for to simulate evaporation in the model. Heat transfer within all domains is defined by Eq. (4),

$$Q = \rho C \left(\frac{\partial T}{\partial t} + v \cdot \nabla T \right) - K \nabla^2 T, \tag{4}$$

in which Q is the heat source, C is the heat capacity, v is the velocity, and K is the isotropic thermal conductivity. A Neumann boundary condition was applied on the meniscus surface for heat transfer. The evaporation process was modeled by using the diffusion equation within the air domain,[19,20]

$$\frac{\partial c_v}{\partial t} = D_v \nabla^2 c_v, \tag{5}$$

in which c_v is the vapor concentration and D_v is the diffusivity of water vapor in air. The evaporation flux at the meniscus–air interface is then expressed as

$$J = D \nabla c, \tag{6}$$

in which J is the evaporation flux.[19,20]

Evaporation on the meniscus surface generates a convective flow within the electrolyte which is directed toward the cathode. Fluid dynamics within the electrolyte was modeled by simultaneously solving the Navier–Stokes and continuity equations, which, respectively, are

$$\rho \left(\frac{\partial u}{\partial t} + u \cdot \nabla u \right) = -\nabla p + \nabla \cdot \left(\mu (\nabla u + (\nabla u)^T) \right) + F, \tag{7}$$

$$\nabla \cdot u = 0, \tag{8}$$

in which u is the fluid velocity, p is the fluid pressure, ρ is the fluid density, μ is the dynamic viscosity of the fluid, and F accounts for external body forces acting on the fluid (e.g., gravity).

FINITE ELEMENT ANALYSIS

Numerical simulations were conducted in the COMSOL Multiphysics software package. A 3D FE model was generated to simulate the parallel CED metal printing process for a 3×3 nozzle array (nine nozzles in total). The model geometry is shown in Figs. 1(a) and 1(b), which represents an array of nine nozzles filled with an aqueous electrolyte of the metal to be deposited (Cu in this case). A single nozzle with the applied boundary conditions is shown in Fig. 1(c). The same boundary conditions were applied to

FIG. 1. (a) A CAD rendering of the 3 × 3 nozzle array, (b) a cross-sectional view of the array, and (c) a close-up view of a single nozzle tip with the applied boundary conditions. The same boundary conditions were applied to all nozzles. The contours for the meniscus surface and meniscus height are shown in Fig. S1 in the supplementary material.

each nozzle within the array. Given the geometric symmetry, only one quarter of the array was modeled to simulate the process. A Cartesian coordinate system was used, in which the x and y axes are in the lateral direction and the z axis is in the vertical direction. The growth angle (φ_0) of the deposited wire was defined as the equilibrium angle between the growth direction and the contact line at the solid–liquid–gas (metal–electrolyte–air) interface. Previous computational studies have used a value of $\varphi_0 = 12^\circ$ for the copper–electrolyte–air system,[16,17,21] which was determined experimentally in Ref. 13.

The relationship between the meniscus height and the diameter of the deposited wire is expressed as

$$H(D) = \frac{1}{2} D \cos\,\varphi_0 \left(\cos\,h^{-1} \frac{D_0}{D \cos\,\varphi_0} - \cos\,h^{-1} \frac{1}{\cos\,\varphi_0} \right), \tag{9}$$

in which D and D_0 are the diameters of deposited wire and nozzle tip, respectively, φ_0 is the growth angle, and $H(D)$ is the meniscus height.[13] A previous computational study has shown that stable deposition occurs within the range of $0.5D_0 \leq D \leq 0.9D_0$, in which $D_{min} = 0.5D_0$ and $D_{max} = 0.9D_0$. Both the diameter of the deposited wire and the height of the meniscus are dependent on v_{dep}, with D_{min} occurring at $v_{dep,\ max}$ and D_{max} occurring at $v_{dep,\ min}$.[17] If the deposition rate is under v_{min}, the wire growth front will quickly reach the nozzle tip and clog the nozzle; and if the deposition rate is over v_{max}, the electrolyte meniscus will break and deposition will cease. In this work, a value of $D_0 = 20\,\mu$m was used in conjunction with v_{min}, resulting in a deposited wire diameter of $D = 18\,\mu$m. The shape of the meniscus during stable growth is then defined as

$$z(r) = \frac{1}{2} D \cos\,\varphi_0 \left(\cos\,h^{-1} \frac{D_0}{D \cos\,\varphi_0} - \cos\,h^{-1} \frac{2r}{D \cos\,\varphi_0} \right), \tag{10}$$

in which r is the coordinate point in the lateral direction between the outer edge of the deposited wire and the outer edge of the nozzle tip.[13,22] A parametric study on nozzle length showed that results were not affected when the length of the nozzle was large enough compared to meniscus height. Thus, the nozzle length was set to be $100\,\mu$m in the simulation.

The electrolyte of interest is copper sulfate (CuSO$_4$), which is contained in a glass nozzle in an air environment with controlled humidity. Simulation of the CED process was divided into two steps: in the first stationary step, evaporation on each meniscus surface was calculated by solving the heat transfer and diffusion equations. Evaporation was treated as a time-independent process since no environmental changes occur. In a subsequent time-dependent step, the calculated evaporation rate on each meniscus surface served as the outlet velocity for the electrolyte.

The transport of the electrolyte solution was modeled by coupling the Nernst–Planck equation with the Navier–Stokes equation. There is no flux through the walls of the nozzle as they are insulated. A no-slip condition was also applied on the internal nozzle walls. Parameters and boundary conditions in the model were applied based on previous studies and experimental conditions.[16,17] Atmospheric pressure and room temperature were assumed for all domains within the model. A bulk electrolyte concentration of 10 mol/m^3 was used in conjunction with electrolyte viscosity and density of 0.0010093 Pa s and 1000 kg/m^3, respectively. Furthermore, diffusivity of Cu^{2+} ions was assumed to be 5×10^{-10} m^2/s.[23] Values used in Eq. (2) were $i_0 = 30\,\frac{A}{m^2}$, $\alpha_a = 0.5$, $\alpha_c = 1.5$, $C_O = \frac{C_{Cu^{2+}}}{C_{Cu^{2+}_{ref}}}$, and $C_R = 1$, in which $C_{Cu^{2+}}$ and $C_{Cu^{2+}_{ref}}$ are the concentrations of Cu^{2+} ions on the cathode surface and in the bulk electrolyte, respectively.[24,25] A potential difference of 0.4 V was applied between the anode and the cathode. According to a previous study,[13] an environmental relative humidity of 70% falls near the middle of the applicable experimental range of values and provides ideal conditions for stable wire growth. Thus, all simulations were performed using this value.

RESULTS AND DISCUSSION

The presented FE model was used to investigate the effects of nozzle spacing on metal deposition rate in the parallel CED process. Twelve different values for tip spacing were considered in the analysis, specifically 1, 5, 10, 20, 30, 40, 50, 60, 70, 80, 90, and $100\,\mu$m. Here, we defined the tip spacing as the lateral distance

Published under an exclusive license by AIP Publishing

between nozzle tips. The results were analyzed for each individual nozzle within the array. Each nozzle is numbered in Fig. 2(a) for use in subsequent analysis. In the numbering, we considered the symmetry in the model. The material deposition rate (V_{dep}) on the cathode surface for each nozzle was first calculated for each tip spacing value, as it is of interest to determine the relationship between the tip spacing and the average deposition rate for all nozzles (numbered 1, 2, and 3). We calculated V_{dep} by integrating the metal deposition over the entire nozzle tip surface (cathode). Interestingly, we found that insufficient evaporation on each meniscus surface will occur if the nozzles are too close together, primarily due to less exposure to the ambient air environment. This results in non-uniform metal deposition among nozzles and, thus, non-uniform geometries of the final printed structures.

As an example, the contour plot of growth rate on the surface of each cathode for a tip spacing of 50 μm is shown in Fig. 2(b). As nozzle 3 has the most exposure to the environment and, thus, the highest deposition rate, the deposition rates for nozzles 1 and 2 were normalized by the deposition rate for nozzle 3. Such data are shown in Fig. 2(c).

The plot shown in Fig. 2(c) can be roughly divided into two regions: (i) tip spacing <50 μm and (ii) tip spacing >50 μm. The deposition rate ratio increases for both nozzles 1 and 2 within region (i) because of increased exposure to the surrounding air. Both ratios become near constant within region (ii) once a spacing of ∼50 μm is reached, with ratios for deposition rate for nozzle 1/nozzle 3 and nozzle 2/nozzle 3 approaching values of ∼0.85 and ∼0.93, respectively. More specifically, the growth rate for nozzle 1 reaches a maximum value of ∼85% of the growth rate for nozzle 3, while the growth rate for nozzle 2 reaches a maximum value of ∼93% of that for nozzle 3. Thus, it becomes increasingly less beneficial to increase tip spacing beyond 50 μm if the goal is to equalize deposition rates of all nozzles, while printing metal structures with high spatial resolution. Of course, the exception would be if a

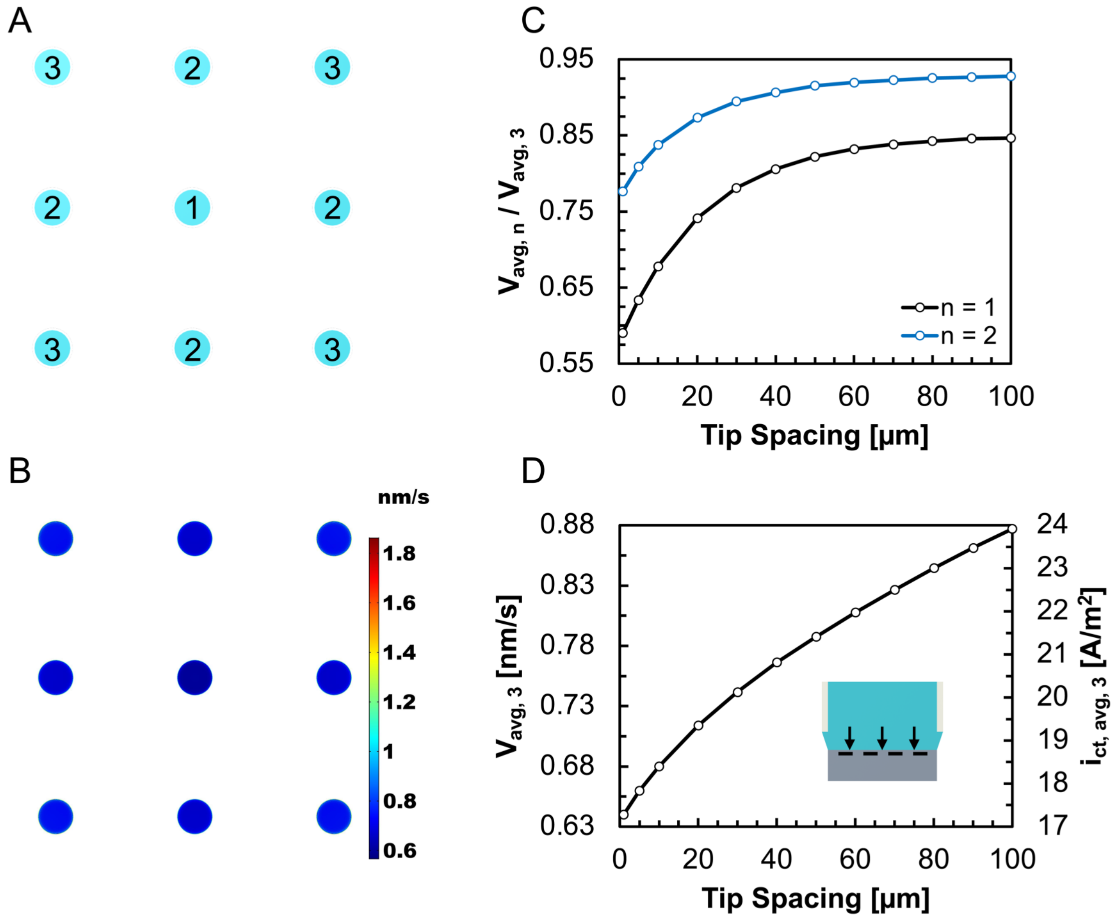

FIG. 2. (a) A top view of the nozzle array. Each nozzle is numbered for use in subsequent data analysis. (b) The deposition rate on the cathode surfaces for a tip spacing of 50 μm. (c) The ratio of the average deposition rate for nozzle 1/nozzle 3 and nozzle 2/nozzle 3 as a function of tip spacing. Average deposition rates for nozzles 1 and 2 were normalized by that of nozzle 3, as nozzle 3 has the most exposure to the ambient air environment and thus the highest deposition rate. (d) The average deposition rate and current density for nozzle 3 as a function of tip spacing.

Published under an exclusive license by AIP Publishing

particular application requires relatively large areas of free space between structures. Furthermore, the obtained growth rates in Fig. 2(b) follow the trend of values reported in Ref. 17. Although the nozzle diameter in this work is 20 μm, at a tip spacing of 50 μm, the average deposition rates were calculated as 0.65, 0.72, and 0.79 nm/s for nozzles 1, 2, and 3, respectively. As the nozzle diameter increases, the evaporation and deposition rate decrease due to decreasing meniscus surface area-to-volume ratio (A/V). The surface area-to-volume ratio for various nozzle diameters is shown in Fig. S2 in the supplementary material. A/V sharply reduces as the nozzle diameter increases. For example, A/V for a 0.25 μm nozzle is ∼18.4 μm^{-1}, A/V for a 1 μm nozzle is ∼4.6 μm^{-1}, and A/V for a 20 μm nozzle is ∼0.23 μm^{-1}.

It has been established that for small diameter nozzles with high A/V ratio, evaporation drives the CED process and deposition rate is a direct product of the evaporation rate on the meniscus surface.[16,17] We calculated the average evaporation rate (AER) on each meniscus surface, and the AER on meniscus surfaces for nozzles 1 and 2 were each normalized by that of nozzle 3. Figure 3(a) displays the relative humidity within the air domain surrounding the nozzles. Figure 3(b) shows the AER ratio for tip spacings in the range of 1–100 μm. We found that the AER plateaus once a tip spacing of ∼50 μm is reached, similar to the plot for deposition rate ratio in Fig. 2(c). The AER on nozzle 1′s meniscus surface approaches ∼79% of the AER on nozzle 3′s meniscus surface, while the AER on nozzle 2′s meniscus surface approaches ∼90% of that for nozzle 3.

Both the evaporation rate and deposition rate are relatively low despite ratios of the two becoming near constant at tip spacings of ≥50 μm. At a tip spacing of 50 μm and relative humidity of 70%, the AER for nozzle 3 was found to be 0.016 mm/s, compared to an AER of 0.8 mm/s for a single 0.86 μm nozzle reported in Ref. 16. Furthermore, the average deposition rate for nozzle 3 was found to be 0.79 nm/s, compared to a value of approximately 70 nm/s for the 0.86 μm diameter nozzle. We found that the low deposition rate is a direct result of insufficient evaporation on the meniscus surface. Furthermore, altering the humidity of the environment has a little effect at this scale (of nozzle diameters). For example, at a relative humidity of 10% and tip spacing of 50 μm, the average evaporation and deposition rates for nozzle 3 were found to be 0.047 and 2 nm/s, respectively, as shown in Fig. S3 in the supplementary material. Although higher than both values for the case of 70% relative humidity, the evaporation rate is still too low to result in desirable deposition rates. Additionally, this value is well outside the appropriate experimental humidity range of 60%–80%.[16] Thus, we conclude that a low humidity alone is not suitable to induce sufficient convection and desirable metal deposition for a 20 μm nozzle, particularly in the case of a 3 × 3 array.

To counteract the low evaporation rate for the 20 μm nozzle array, we introduced a flow rate at the inlet of the fluid reservoir to enhance convection within the electrolyte. This flow rate essentially simulates an external pump, which is used experimentally for "larger" nozzles.[26–28] In this simulation, there is no need for the air domain and the stationary step, in which heat transfer and evaporation were calculated. All other boundary conditions and geometries remained the same and a tip spacing of 50 μm was used. To determine the effects on the Cu deposition rate, we examined a series of reservoir inlet flow rates between 0.025 and 2.5 nl/s. The flow rates were set at the inlet of the entire reservoir, as shown in Fig. 1(a).

As shown in Fig. 4, the ionic concentration within the meniscus changes drastically depending on the inlet flow rate of the reservoir. Particularly in the case of a flow rate of 2.5 nl/s, we found that the concentration is considerably higher than that of the bulk electrolyte (10 mol/m^3), particularly on the meniscus surface. References 16 and 17 have reported such a change in concentration due to strong diverging convective flux, specifically because fluid flow is directed toward the top corner of the meniscus. Our results show that this phenomenon results in discrepancies between

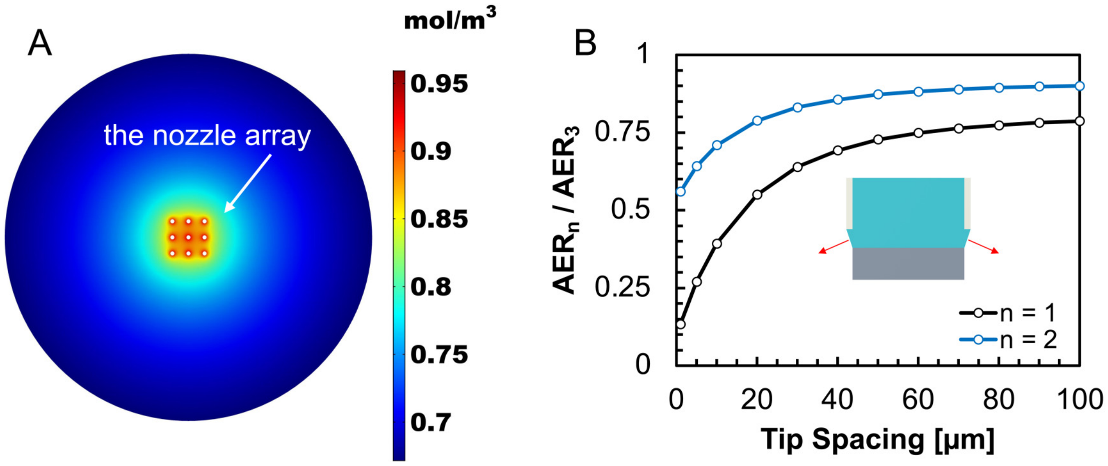

FIG. 3. (a) The relative humidity within the vicinity of the nozzles as observed from the bottom of the array. In this case, the environment humidity was set to 70%. (b) The ratio of the average evaporation rate (AER) for nozzle n/nozzle 3 (n = 1, 2) as a function of tip spacing. AERs for nozzles 1 and 2 were normalized by that of nozzle 3, as nozzle 3 has the most exposure to the ambient air environment.

Published under an exclusive license by AIP Publishing

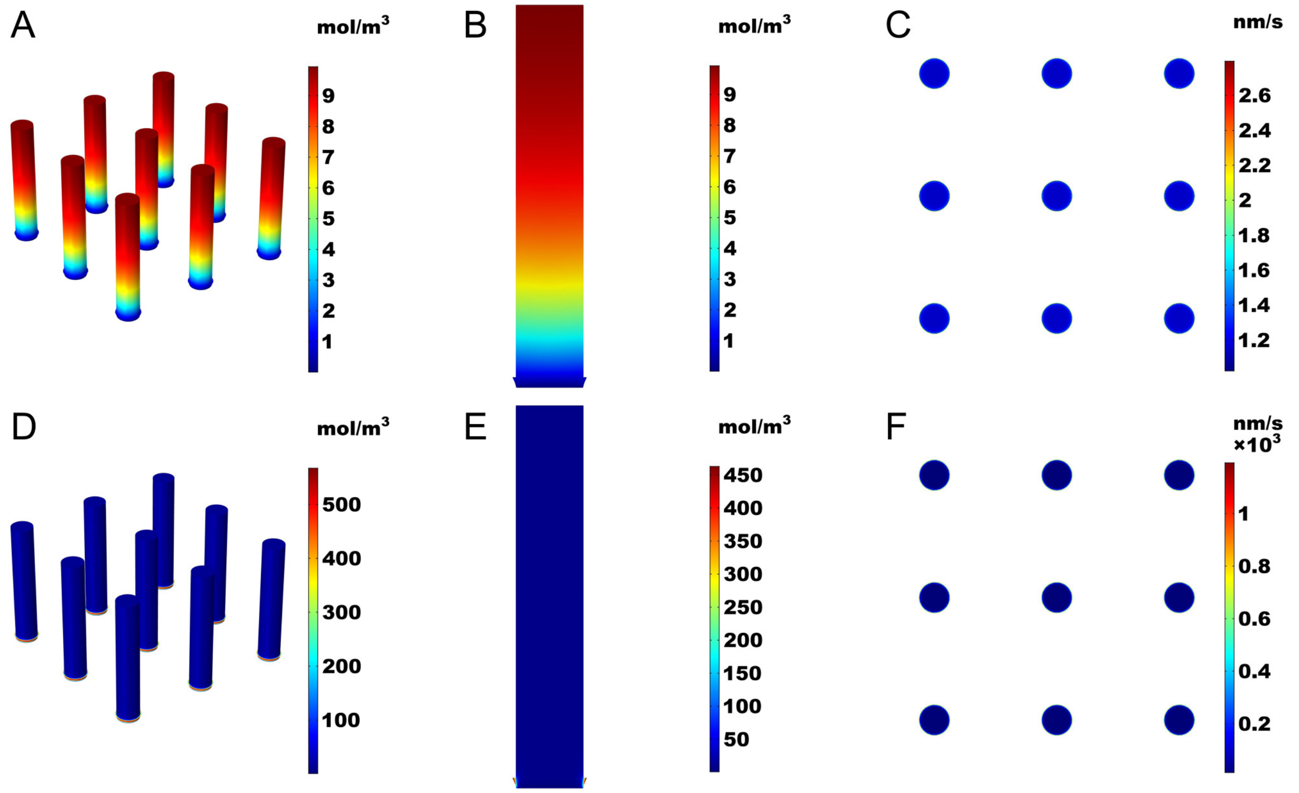

FIG. 4. Electrolyte concentration in (a) the nozzle array and (b) the center nozzle for an inlet flow rate of 0.05 nl/s. (c) Growth rate on the cathode surfaces for an inlet flow rate of 0.05 nl/s. Electrolyte concentration in (d) the nozzle array and (e) the center nozzle for an inlet flow rate of 2.5 nl/s. (f) Growth rate on the cathode surfaces for an inlet flow rate of 2.5 nl/s. The fluid reservoir is not shown so all nozzles are viewable.

material deposition at the center of each nozzle and the edge of each nozzle. The deposition rates for inlet flow rates of 0.05 and 2.5 nl/s are shown in Figs. 4(c) and 4(f). For a flow rate of 0.05 nl/s, the deposition rate at the center of each nozzle is ∼48% of that at the edge of each nozzle; and this deposition is relatively uniform. However, for a flow rate of 2.5 nl/s, the deposition rate at the center of each nozzle is ∼1.8% of that at the edge of each nozzle, which will result in thin-walled, hollow structures. This is shown further in Figs. 4(c) and 4(f).

Comprehensive data for all examined flow rates between 0.025 and 0.5 nl/s are shown in Fig. 5. To further investigate the effects of the inlet flow rate on deposition rate, we calculated the ratio of deposition rate at the center of each nozzle to the edge of each nozzle ($V_{dep,\ center}/V_{dep,\ edge}$). Our results show that the deposition ratio is inversely proportional to the flow rate, while the average deposition rate is proportional to the flow rate. However, the higher average deposition rate comes at the drawback of geometric non-uniformity; and at a flow rate of 2.5 nl/s, copper will be deposited nearly 57 times faster at the edge of the nozzle compared to the center. Thus, a flow rate of 0.025 nl/s is ideal to print relatively uniform structures at the drawback of slower deposition. Although the evaporation is not present, an external pump can provide sufficient convection to achieve relatively large deposition rates compared to the model with evaporation. Additionally, the thickness of the printed structure can be tailored by simply changing the inlet flow rate.

To determine its relation to the deposition rate, we calculated the average ionic concentration within the meniscus as a function of the flow rate. Furthermore, the contributions of each transport mechanism (diffusion, convection, and migration) to the total flux at the tip of each nozzle were calculated as a function of the inlet flow rate. Reference 17 reported that back diffusion of the electrolyte will occur if the electrolyte meniscus concentration is higher than that of the bulk electrolyte (10 mol/m^3), particularly if using nozzles with diameter ≤700 nm due to relatively large A/V and evaporation rate. This is not an issue if relying on evaporation for nozzles with larger diameters due to an exponentially decreasing A/V. Surprisingly, we found that this phenomenon can occur in larger nozzles if the electrolyte is pumped too fast. Based on Fig. 6(a), we found that back diffusion will begin to occur (particularly at the top corner of each meniscus) at a flow rate of ∼1.125 nl/s. This can further be observed in Fig. 6(b). The contribution of convection to total flux surpasses 100% once a flow rate of ∼1.125 nl/s is reached, with diffusion contributing 0% to ion transport. Convection and diffusion continue to increase and decrease, respectively, as the flow rate increases. We found that

Published under an exclusive license by AIP Publishing

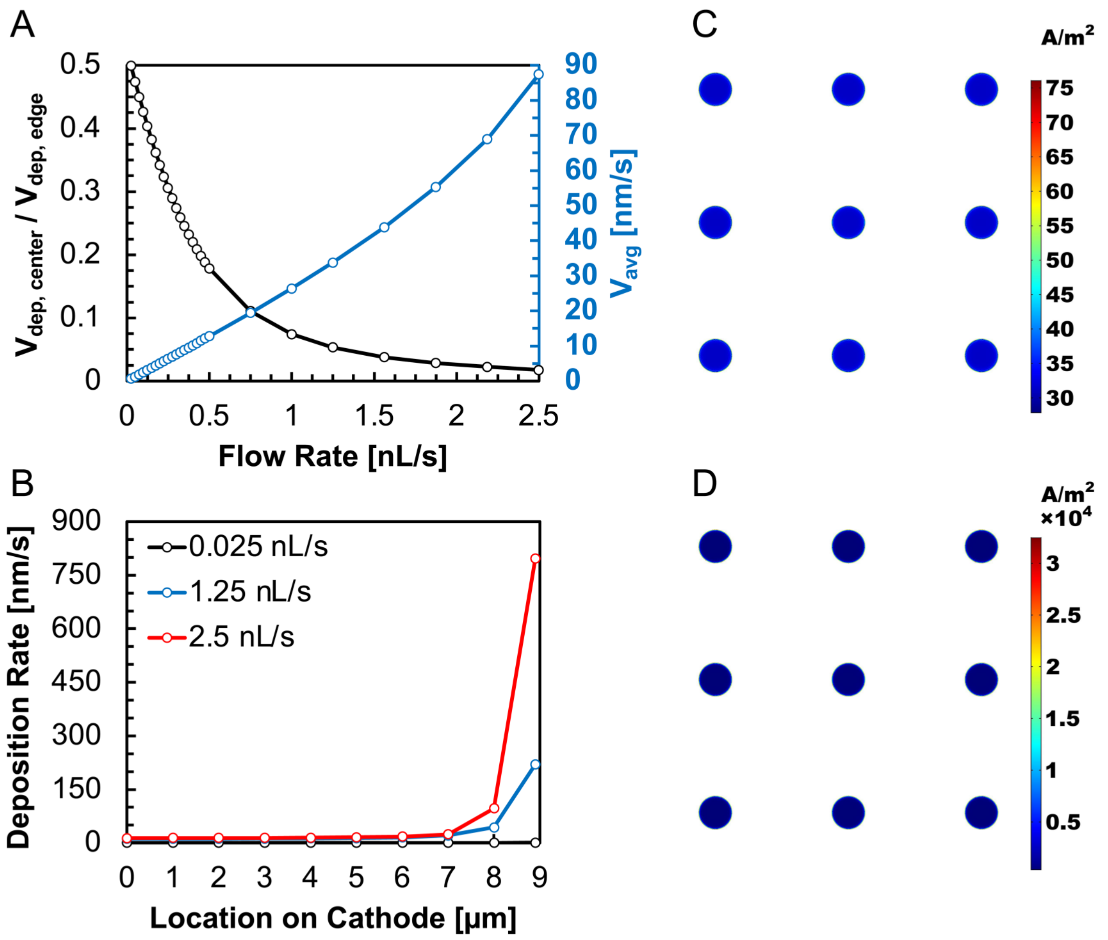

FIG. 5. (a) The ratio of deposition rate at the center and edge of each nozzle and the average deposition rate as a function of inlet flow rate. (b) The variation of deposition rate on the cathode surfaces for different inlet flow rates. Average current density on the cathode surface for an inlet flow rate of (c) 0.05 and (d) 2.5 nl/s.

convection accounts for nearly 220% of total flux at a maximum tested flow rate of 2.5 nl/s, whereas diffusion accounts for −35% of total flux. As shown previously in Figs. 4(f) and 5(b), deposition varies drastically between the center and edge of each nozzle; and this is a direct result of fluid transport being convection driven. Thus, we conclude that increasing convection within the electrolyte will result in non-uniform, thin-walled structures. Flow rates of below 1.125 nl/s should be used to obtain better uniformity of printed structures.

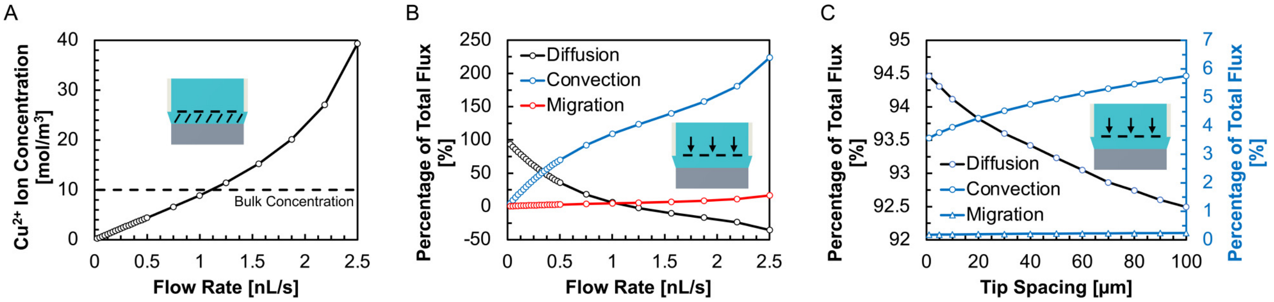

FIG. 6. (a) The average concentration of Cu^{2+} ions within the meniscus as a function of the inlet flow rate. (b) Contribution of each transport mechanism as a function of inlet flow rate. (c) Contribution of each transport mechanism as a function of tip spacing with evaporation present.

Published under an exclusive license by AIP Publishing

CONCLUSIONS

Overall, a Multiphysics FE model was developed to investigate and optimize the CED process for an array of microscale nozzles. Based on simulation results, evaporation alone is not suitable for "fast" or uniform deposition due to the relatively low meniscus surface area-to-volume ratio. Additionally, we found that it becomes increasingly less beneficial to increase tip spacing beyond 50 μm if relying on evaporation to drive the process. Once this point is reached, deposition is still highly non-uniform between nozzles due to insufficient exposure to the ambient air environment. However, our results reveal that an external pump can be used to counteract the low evaporation rate and tailor convection within the electrolyte. Depending on the desired application, flow rate can be changed to print structures of varying uniformity at different speeds. However, several challenges remain (1) new nozzle geometries should be developed and studied to achieve both fast and uniform deposition in larger nozzles and (2) larger arrays should be studied to enable higher throughput and efficiency of the printing process. While larger arrays will allow for more structures to be printed simultaneously, a reliance on evaporation alone may increase non-uniformity between inner and peripheral nozzles due to less exposure to the ambient air environment.

SUPPLEMENTARY MATERIAL

See the supplementary material for a close-up image of the nozzle/electrolyte system, the ratio of the surface area-to-volume ration of the meniscus, and the average evaporation rate as a function of relative humidity.

ACKNOWLEDGMENTS

This work was partially supported by National Science Foundation (Grant No. 2152725) and Department of Energy SBIR (Grant No. DE-SC0018905), sub-contract from UHV Technologies, Inc.

AUTHOR DECLARATIONS

Conflict of Interest

The authors do not have any conflicts of interest.

DATA AVAILABILITY

The data that support the findings of this study are available from the corresponding author upon reasonable request.

REFERENCES

[1] J. H. Martin, B. D. Yahata, J. M. Hundley, J. A. Mayer, T. A. Schaedler, and T. M. Pollock, "3D printing of high-strength aluminium alloys," Nature **549**, 365–369 (2017).

[2] E. Uhlmann, R. Kersting, T. B. Klein, M. F. Cruz, and A. V. Borille, "Additive manufacturing of titanium alloy for aircraft components," Proc. CIRP **35**, 55–60 (2015).

[3] L. E. Murr, "Frontiers of 3D printing/additive manufacturing: From human organs to aircraft fabrication," J. Mater. Sci. Technol. **32**(10), 987–995 (2016).

[4] J. Ni *et al.*, "Three-dimensional printing of metals for biomedical applications," Mater. Today Bio **3**, 100024 (2019).

[5] S. Cooke, K. Ahmadi, S. Willerth, and R. Herring, "Metal additive manufacturing: Technology, metallurgy, and modelling," J. Manuf. Processes **57**, 978–1003 (2020).

[6] D. Zhang *et al.*, "Metal alloys for fusion-based additive manufacturing," Adv. Eng. Mater. **20**(5), 1700952 (2018).

[7] X. Song, W. Zhai, R. Huang, J. Fu, M. Fu, and F. Li, "Metal-based 3D-printed micro parts and structures," in *Reference Module in Materials Science and Materials Engineering* (Elsevier Inc., 2020), pp. 1–14.

[8] W. E. Frazier, "Metal additive manufacturing: A review," J. Mater. Eng. Perform. **23**(6), 1917–1928 (2014).

[9] N. Zhou, C. Liu, J. A. Lewis, and D. Ham, "Gigahertz electromagnetic structures via direct ink writing for radio-frequency oscillator and transmitter applications," Adv. Mater. **29**(15), 1601598 (2017).

[10] X. Ruan *et al.*, "Emerging applications of additive manufacturing in biosensors and bioanalytical devices," Adv. Mater. Technol. **5**(7), 2000171 (2020).

[11] S. Chizari *et al.*, "Current challenges and potential directions towards precision microscale additive manufacturing—Part III: Energy induced deposition and hybrid electrochemical processes," Precis. Eng. **68**, 174–186 (2021).

[12] L. Hirt, A. Reiser, R. Spolenak, and T. Zambelli, "Additive manufacturing of metal structures at the micrometer scale," Adv. Mater. **29**(17), 1604211 (2017).

[13] J. Hu and M. Yu, "Meniscus-confined three-dimensional electrodeposition for direct writing of wire bonds," Science **329**(5989), 313 (2010).

[14] Y. Lin, Y. Zhang, and M. Yu, "Parallel process 3D metal microprinting," Adv. Mater. Technol. **4**(1), 1800393 (2019).

[15] Y. Lin, "Precision 3-D metal microstructure array fabrication with direct-write electrodeposition," Ph.D. dissertation (School of Mechanical Engineering, Georgia Institute of Technology, 2017).

[16] S. Morsali *et al.*, "Multi-physics simulation of metal printing at micro/nanoscale using meniscus-confined electrodeposition: Effect of environmental humidity," J. Appl. Phys. **121**(2), 024903 (2017).

[17] S. Morsali *et al.*, "Multi-physics simulation of metal printing at micro/nanoscale using meniscus-confined electrodeposition: Effect of nozzle speed and diameter," J. Appl. Phys. **121**(21), 214305 (2017).

[18] H. Xiao, P. Zeng, X. Ren, and F. Wang, "Three-dimensional microfabrication of copper column by localized electrochemical deposition," in *2016 17th International Conference on Electronic Packaging Technology (ICEPT)* (IEEE, 2016).

[19] R. Bhardwaj, X. Fang, and D. Attinger, "Pattern formation during the evaporation of a colloidal nanoliter drop: A numerical and experimental study," New J. Phys. **11**, 075020 (2009).

[20] R. Mollaret, K. Sefiane, J. R. E. Christy, and D. Veyret, "Experimental and numerical investigation of the evaporation into air of a drop on a heated surface," Chem. Eng. Res. Des. **82**(4), 471–480 (2004).

[21] S. Morsali, D. Qian, and M. Minary-Jolandan, "Mechanisms of localized pulsed electrodeposition (L-PED) for microscale 3D printing of nanotwinned metals," J. Electrochem. Soc. **166**(8), D354–D358 (2019).

[22] V. A. Tataerchenko *et al.*, "Theoretical model of crystal growth shaping process," J. Cryst. Growth **180**(3), 615–626 (1997).

[23] J. T. Hinatsu and F. R. Foulkes, "Diffusion coefficients for copper (II) in aqueous cupric sulfate-sulfuric acid solutions," J. Electrochem. Soc. **136**(1), 125–132 (1989).

[24] T. M. Braun and D. T. Schwartz, "Localized electrodeposition and patterning using bipolar electrochemistry," J. Electrochem. Soc. **162**(4), D180–D185 (2015).

[25] W. Zeng, M. L. Free, and S. Wang, "Simulation study of electrolyte flow and slime particle transport in a newly designed copper electrorefining cell," ECS Trans. **72**(22), 23–42 (2016).

[26] C. Wang, M. E. Hossain Bhuiyan, S. Moreno, and M. Minary-Jolandan, "Direct-write printing copper-nickel (Cu/Ni) alloy with controlled composition from a single electrolyte using Co-electrodeposition," ACS Appl. Mater. Interfaces **12**(16), 18683–18691 (2020).

[27] M. E. Hossain Bhuiyan, S. Moreno, C. Wang, and M. Minary-Jolandan, "Interconnect fabrication by electroless plating on 3D-printed electroplated patterns," ACS Appl. Mater. Interfaces **13**(16), 19271–19281 (2021).

[28] M. E. H. Bhuiyan, A. Behroozfar, S. Daryadel, S. Moreno, S. Morsali, and M. Minary-Jolandan, "A hybrid process for printing pure and high conductivity nanocrystalline copper and nickel on flexible polymeric substrates," Sci. Rep. **9**, 19032 (2019).

Published under an exclusive license by AIP Publishing

Supplementary Information

Multiphysics Simulation of Microscale Copper Printing by Confined Electrodeposition using a Nozzle Array

Scott Burlison[1], Majid Minary-Jolandan[2*]

[1]Department of Mechanical Engineering, The University of Texas at Austin, Austin, TX 78712

[2]Mechanical and Aerospace Engineering, School for Engineering of Matter, Transport and Energy, Arizona State University, Tempe, AZ 85287, USA

* Corresponding author: majid.minary@asu.edu

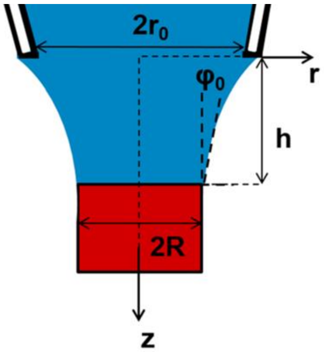

Figure S1 A close-up image of the nozzle / electrolyte system. The variables shown are relevant to those in equations 8 and 9. The image has been taken from [17] in the main text.

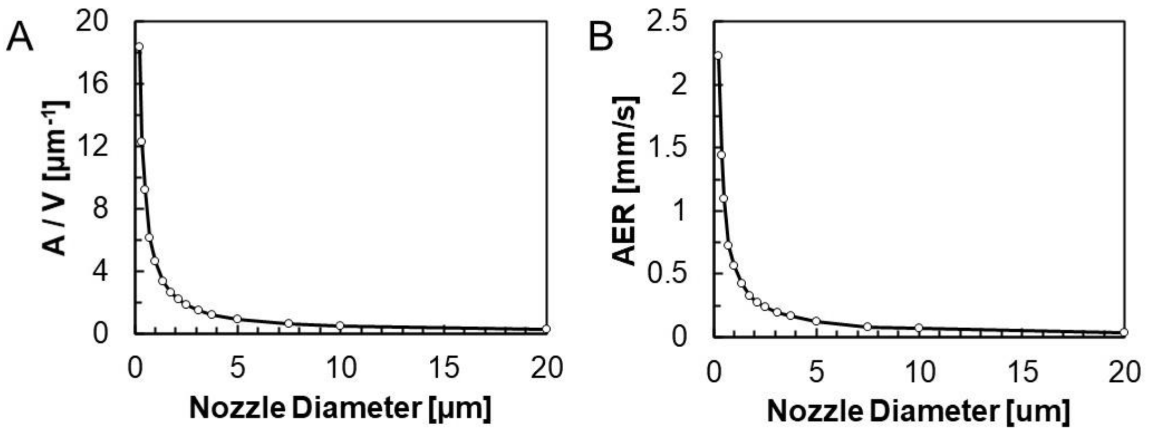

Figure S2 **(A)** The meniscus surface area-to-volume ratio for various nozzle diameters. **(B)** The average evaporation rate on the meniscus surface for various nozzle diameters. The minimum suitable deposition rate ($v_{dep,\ min}$) / maximum deposited wire diameter (D_{max}) were used for all simulations, as defined in the Finite Element Modeling – Geometry section in the article and reference [17].

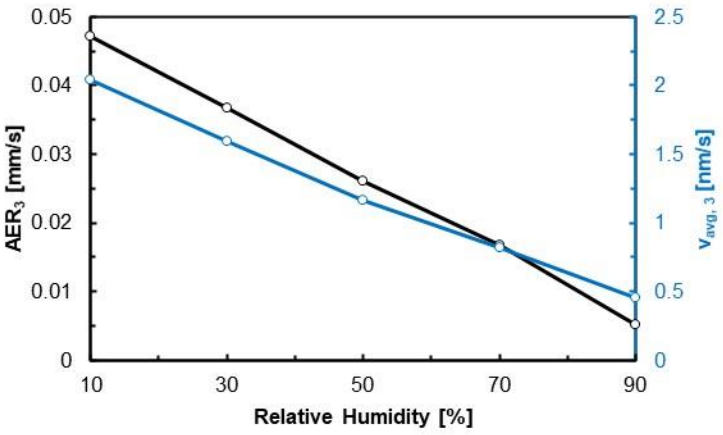

Figure S3 The average evaporation rate (AER) and average deposition rate (V_{avg}) as a function of the relative humidity for nozzle 3. A tip spacing of 50 µm was used for all simulations.